Supplement of Atmos. Chem. Phys., 26, 1145–1161, 2026
https://doi.org/10.5194/acp-26-1145-2026-supplement

Atmospheric Chemistry and Physics
Open Access

Supplement of

Source-resolved volatility and oxidation state decoupling in wintertime organic aerosols in Seoul

Hwajin Kim et al.

Correspondence to: Hwajin Kim (khj0116@snu.ac.kr)

Table S1. Vaporization enthalpy (ΔH_{exp}) and mass accommodation coefficient (α_m) values of each factor resolved by PMF.

PMF factor	Vaporization enthalpy (ΔH_{exp}, kJ mol^{-1}) ($40 \leq \Delta H_{exp} \leq 200$)	Mass accommodation coefficient (α_m) ($0.1 \leq \alpha_m \leq 1$)
HOA	165.86	0.81
COA	161.65	0.79
NOA	167.08	0.82
BBOA	163.84	0.80
LO-OOA	151.57	0.80
MO-OOA	165.00	0.79

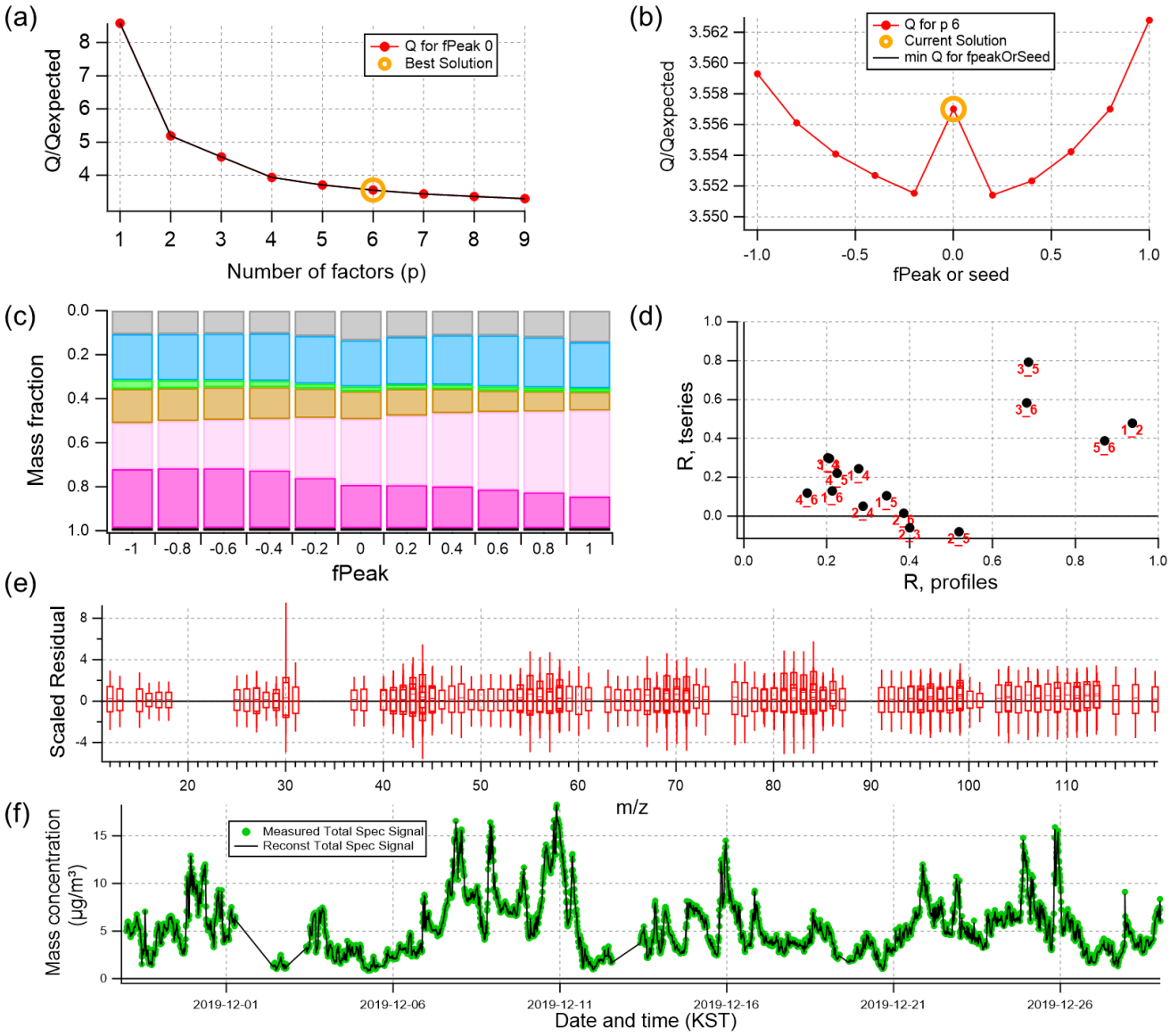

Figure S1. Key diagnostic plots for the six-factor solution resolved by PMF analysis: (a) Q/Q_{exp} against the number of factors (p), (b) Q/Q_{exp} as a function of fPeak, (c) mass fractional contribution of each PMF factor to the total mass, (d) Pearson's r correlation coefficients for correlations among the time series and mass spectra of factors, (e) box and whiskers plot showing the distributions of the scaled residuals for each m/z, (f) time series of the measured mass and the reconstructed mass from the sum of the 6 factors.

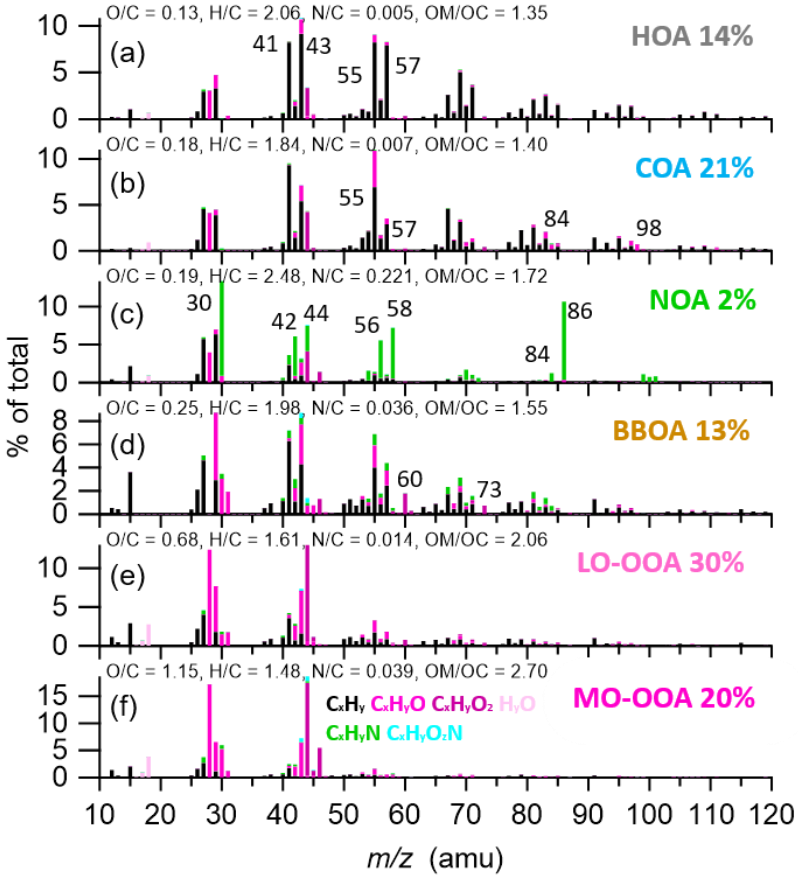

15 **Figure S2.** High-resolution mass spectra of (a) HOA, (b) COA, (c) NOA, (d) BBOA, (e) LO-OOA, and MO-OOA resolved
16 by PMF analysis.

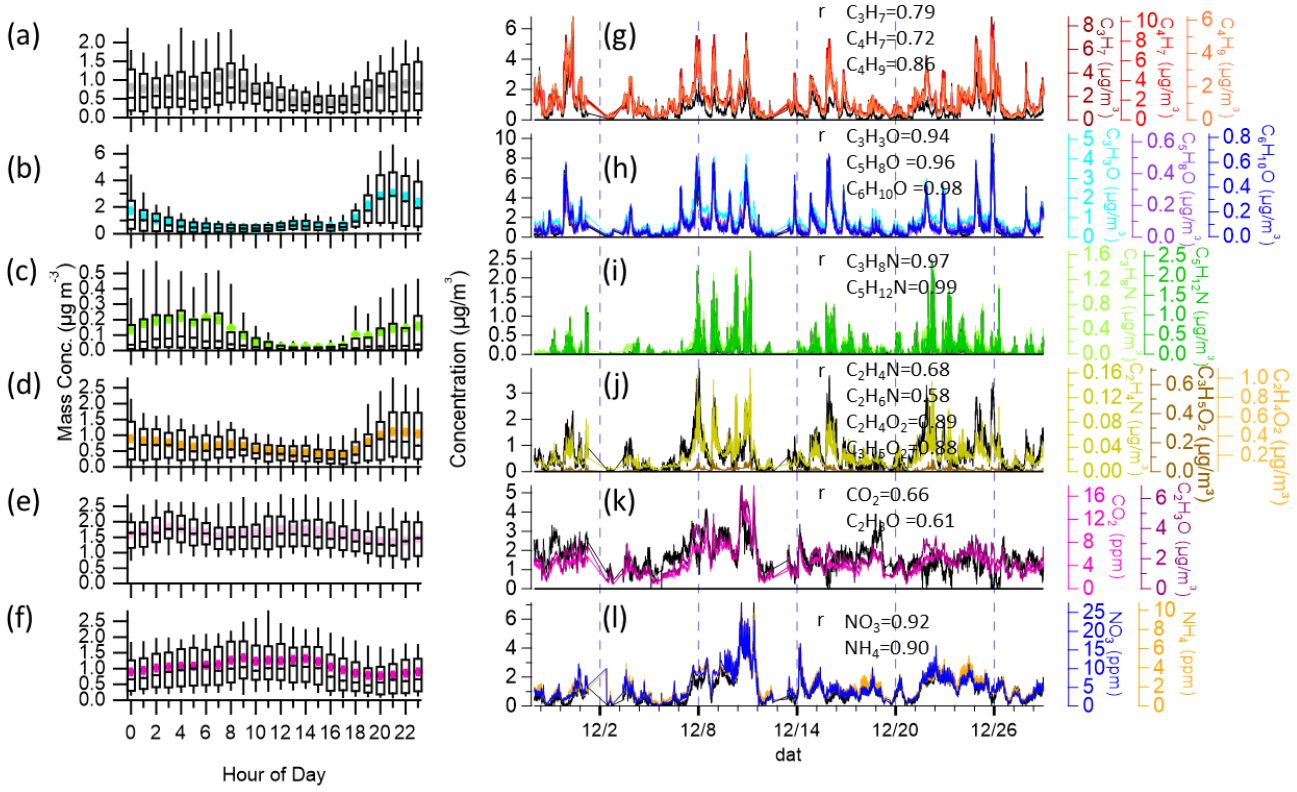

Figure S3. Diurnal variations of (a) HOA, (b) COA, (c) NOA, (d) BBOA, (e) LO-OOA, and (f) MO-OOA resolved by PMF analysis. Comparison of time series and correlations between OA factors (g) HOA, (h) COA, (i) NOA, (j) BBOA, (k) LO-OOA, and (l) MO-OOA and their tracers.

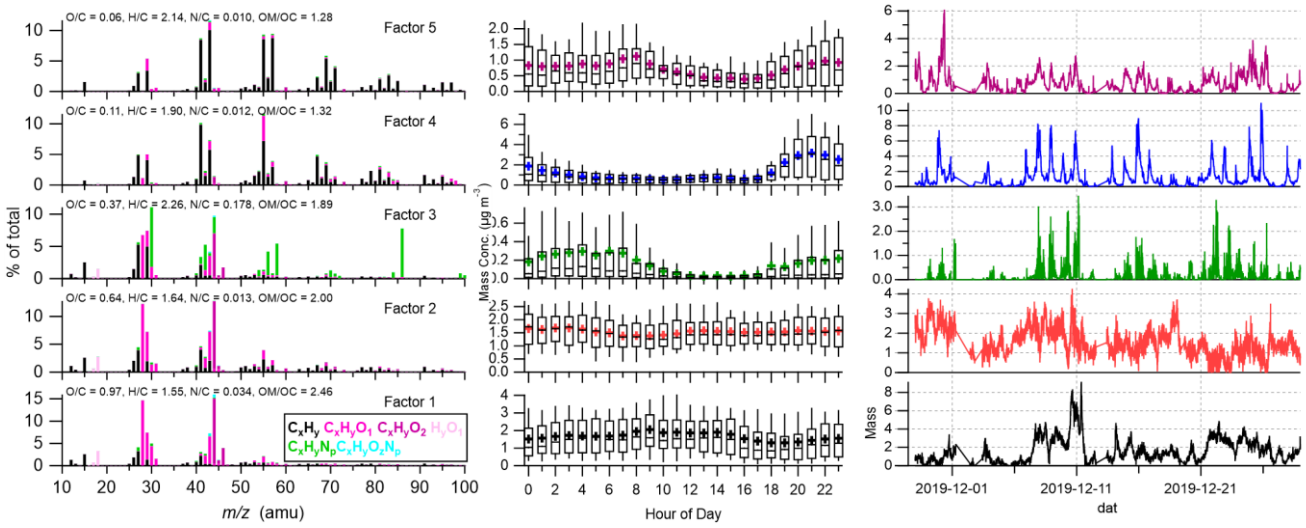

Figure S4. 5-factors result from PMF analysis. The five factors from 1 to 5 are HOA, COA, NOA, LO-OOA, and MO-OOA, respectively.

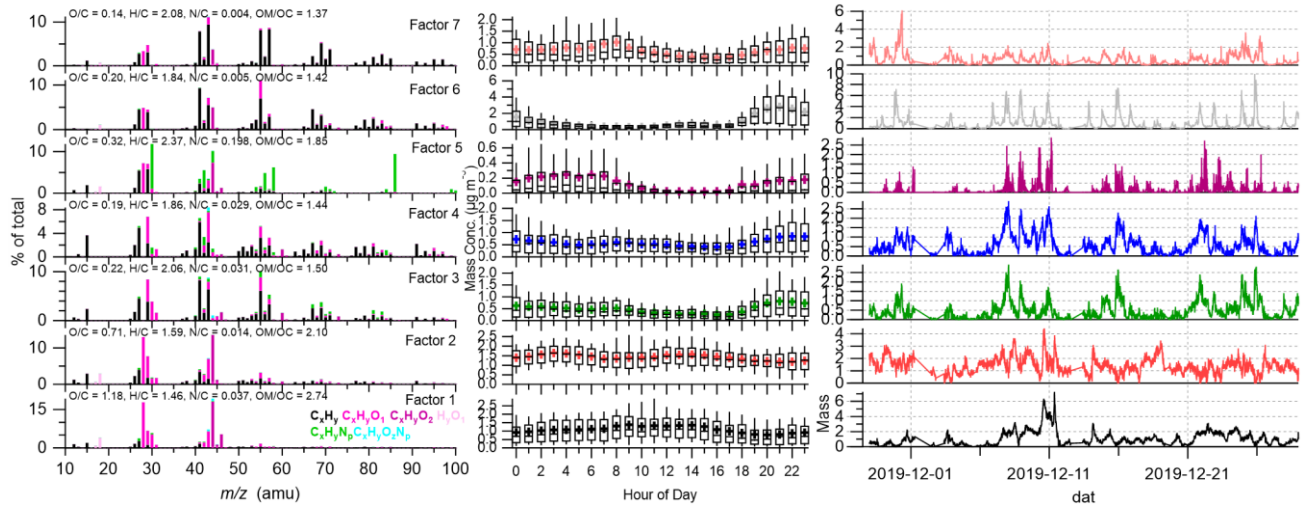

Figure S5. 7-factors result from PMF analysis. The five factors from 1 to 7 are HOA, COA, NOA, BBOA1, BBOA2, LO-OOA and MO-OOA, respectively.

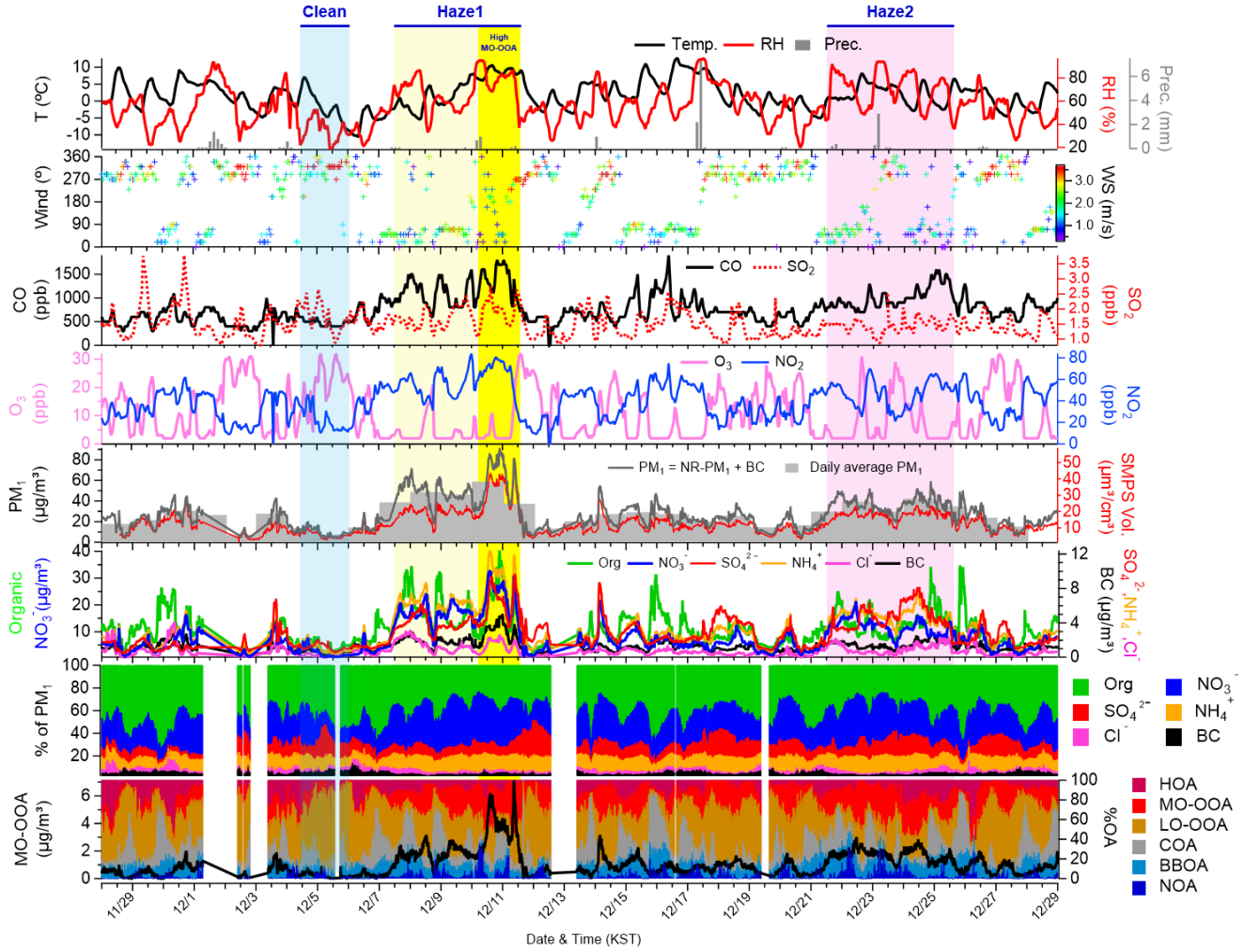

Figure S6. Summary of temporal variations of meteorological variables (Temperature, RH, precipitation, wind direction, and wind speed), gaseous pollutants (CO, SO2, O3, and NO2), PM1, volume concentration from SMPS, NR-species with BC, mass fractional contribution of NR-species with BC and OA, and concentration of MO-OOA. Blue shade indicates a clean period, whereas yellow and pink shades indicate haze periods. The high MO-OOA period is shaded in bright yellow.

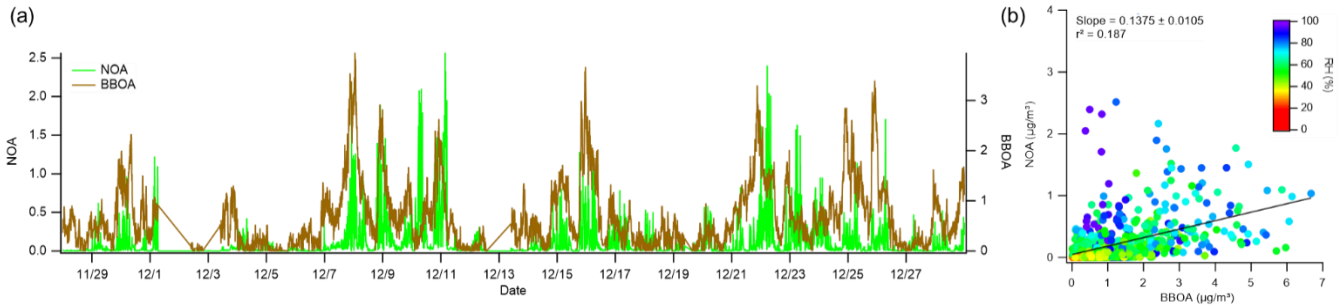

Figure S7. (a) Time series of NOA and BBOA. (b) Scatter plot showing the correlation and slope between NOA and BBOA.

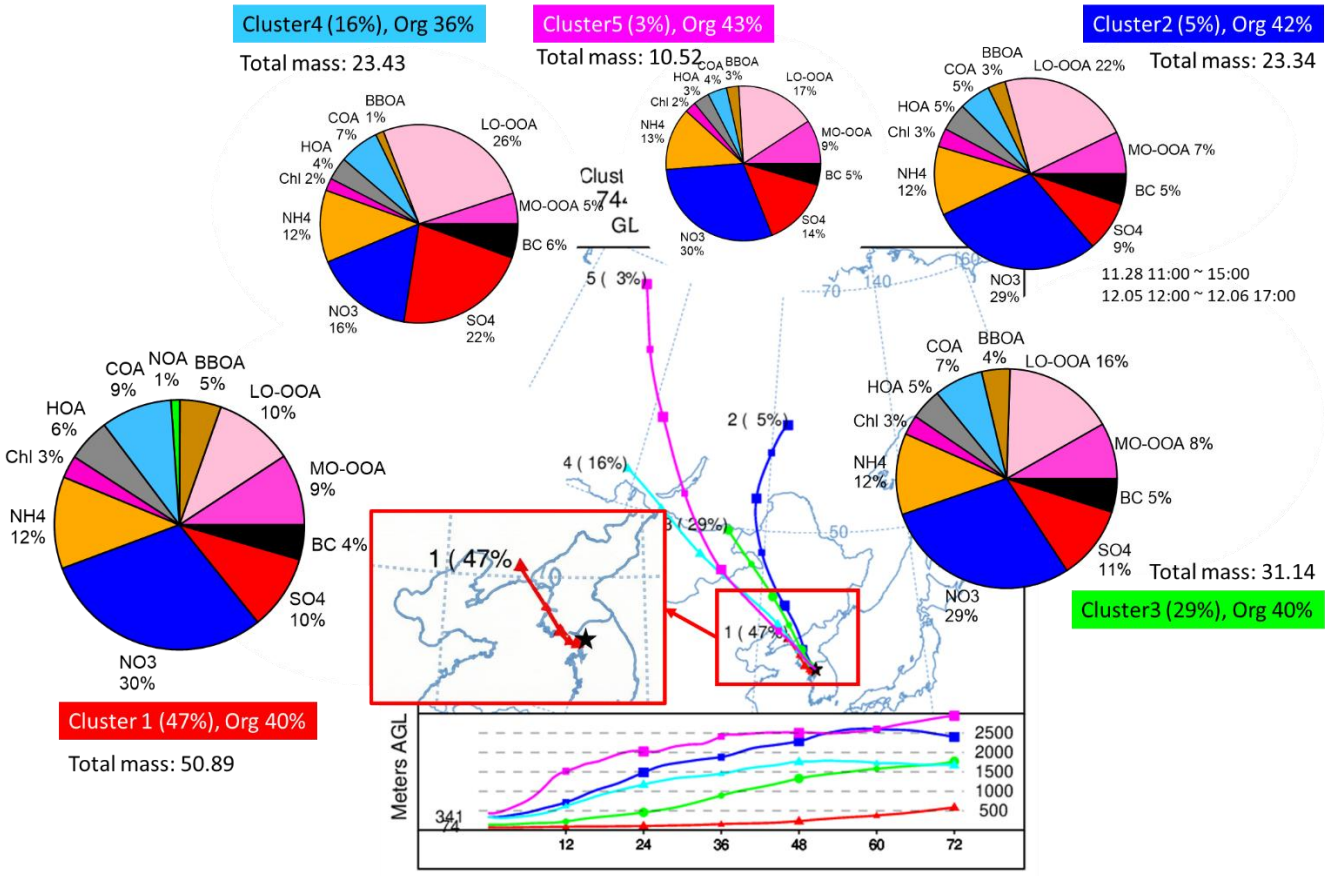

Figure S8. Back trajectories spanning 96 hours were computed hourly using the Hybrid Single-Particle Lagrangian Integrated Trajectory (HYSPLIT; ver 5.0.0b). These trajectories originated from release points set at half of the mixing height at the KIST location (latitude: 37.60° N, longitude: 127.05° E), and on average, the trajectories arrived at an altitude of approximately 191 m (Kim et al., 2017). To discern pollutant properties associated with distinct transport patterns, cluster analysis was conducted on the trajectories using HYSPLIT4 software. Five clusters of trajectories were identified based on their spatial distribution similarities. Five clustered back trajectories; Cluster 1 (47%, total mass: 50.89 μg m^{-3}) from the local area, cluster 2 (5%, total mass: 23.34 μg m^{-3}) from northeast, cluster 3 & 4 (29%, total mass: 31.14 μg m^{-3} & 16%, 23.34 μg m^{-3}) passed through Mongolia and China, and cluster 5 (3%, total mass: 10.52 μg m^{-3}) long-range transfer started from Russia.

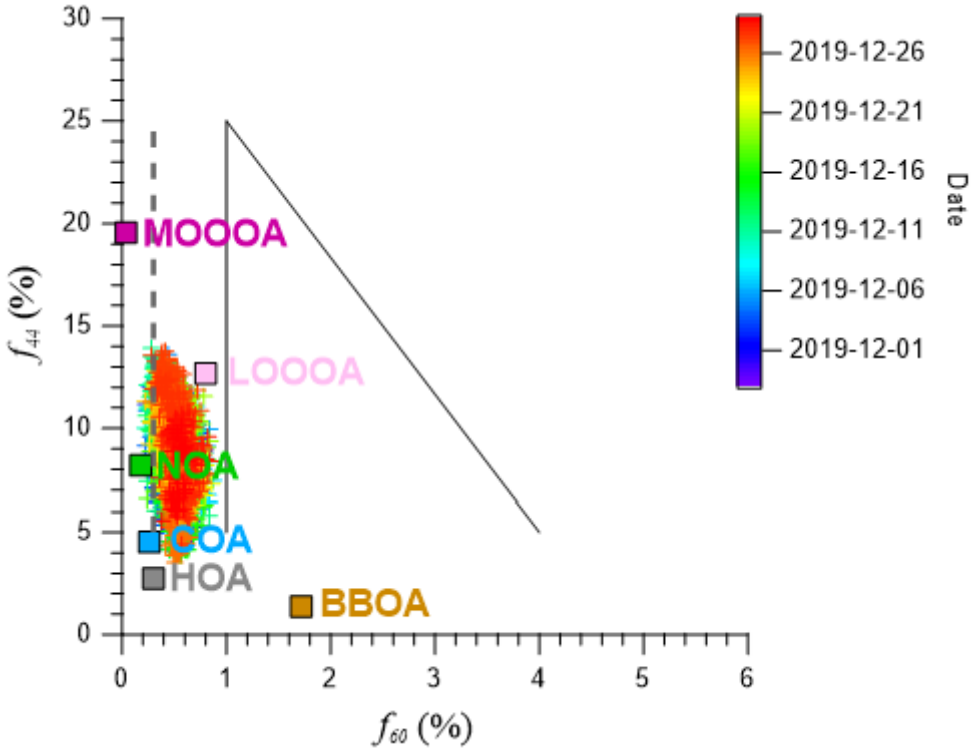

Figure S9. Scatterplots of f_{44} (CO_2^+) vs f_{60} ($C_2H_4O_2^+$)

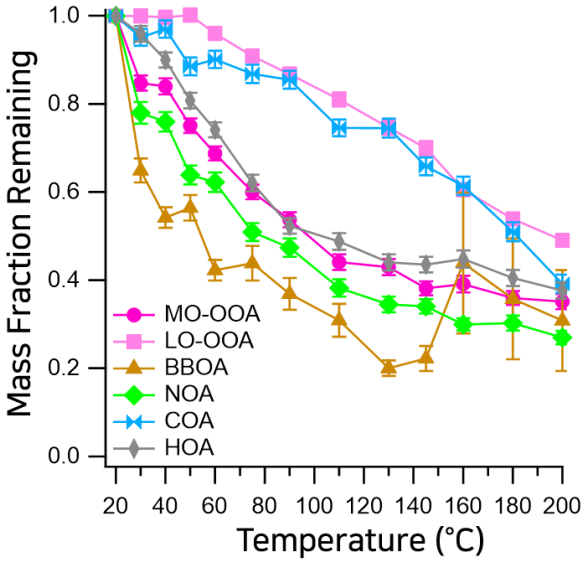

Figure S10. Mass fraction remaining (MFR) of 6 diff erent OA factors resolved by PMF analysis.

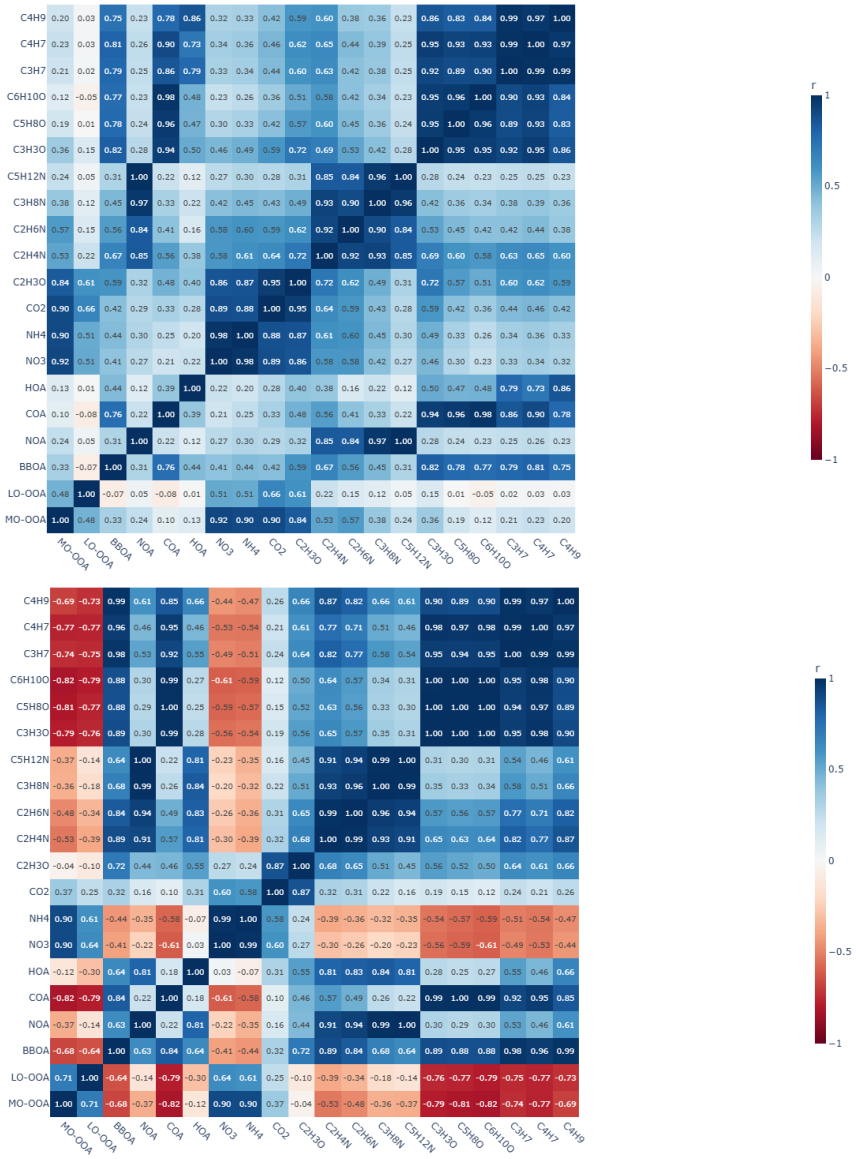

Figure S11. (a)Pearson correlation matrix (*r*) for time-series of six OA factors (HOA, COA, NOA, BBOA, LO-OOA, MO-OOA) and major tracers/ions. Cells show *r* values; stronger positive (negative) correlations appear in darker blue (red). (b). Same as S10a, but for diurnally averaged profiles.

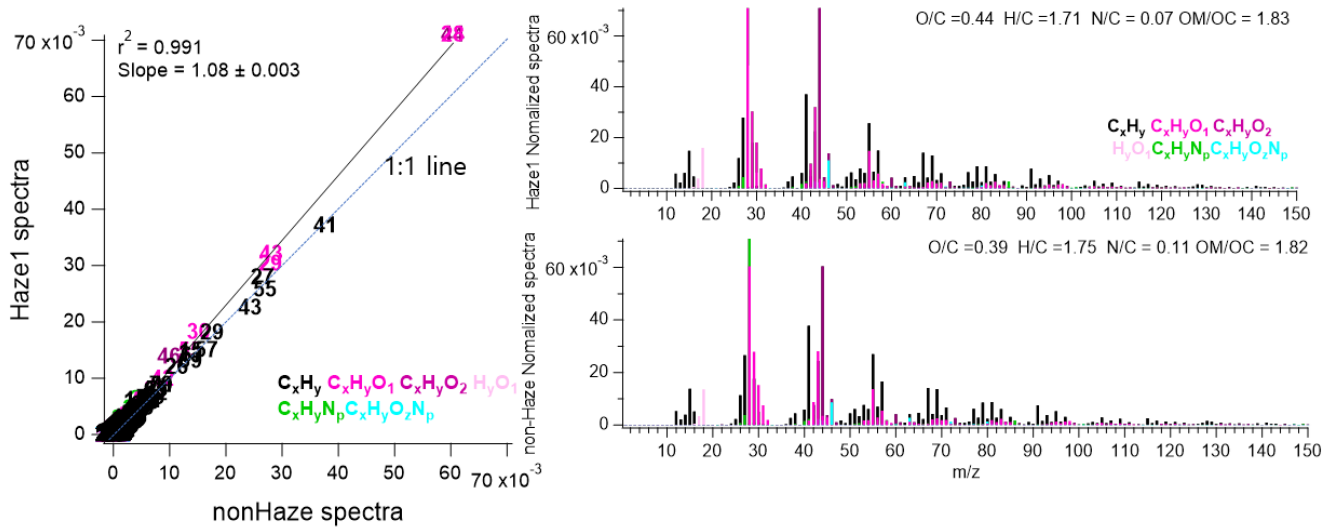

Figure S12. Comparison of organic-aerosol (OA) mass spectra between a haze event and its paired non-haze reference. Left**:** Scatter plot of ion intensities (normalized to OA) for Haze1 vs. non-haze with a 1:1 line (blue). The regression shows strong overall agreement (r^2 = 0.991; slope = 1.08 ± 0.003), with systematic enrichments during haze at oxygenated fragments (*m/z* 28 = CO^+, 29 = CHO^+, 44 = CO_2^+) and a modest relative decrease at hydrocarbon fragments (*m/z* 41, 43, 55, 57). Right, top**:** Haze-1 average spectrum; Right, bottom**:** non-haze average spectrum.

Table S2. Uncertainty in factor concentration for the 5 to 7-factor solution from 100 iterations bootstrap.

	Factor 1	Factor 2	Factor 3	Factor 4	Factor 5	Factor 6	Factor 7
5-factor solution	4.73%	6.46%	5.95%	5.78%	2.59%-	-	-
6-factor solution	4.26% (MO-OOA)	5.23% (LO-OOA)	9.36% (BBOA)	6.48% (NOA)	5.24% (COA)	5.80% (HOA)	-
7-factor solution	5.45%	4.97%	13.32%	7.09%	11.94%	4.85%	6.90%

To ensure the robustness of the 6-factor solution, we calculated uncertainties for each PMF factor using the bootstrap method (100 iterations) with the PET toolkit (v2.05) (EPA, 2014; Xu et al., 2018; Srivastava et al., 2021).

This method generates a time series distribution for each factor, providing an average concentration and standard deviation; the uncertainty is defined as the standard deviation divided by the average concentration.

As shown in Table S2, the 5-factor solution exhibited the lowest average uncertainty (5.10%). While mathematically stable, this low uncertainty is typical of under-resolved solutions where distinct sources are merged. In the 6-factor solution, the average uncertainty increased slightly to 6.06%, with individual factors ranging from 4.26% (MO-OOA) to 9.36% (BBOA). Despite this marginal increase, all factors in the 6-factor solution remained well within the acceptable range (<10%), confirming that the separation of the additional source did not compromise the solution's statistical stability.

In contrast, the 7-factor solution showed signs of instability, with the average uncertainty rising to 7.79% and specific factors exceeding 10% (e.g., Factor 3 at 13.32% and Factor 5 at 11.94%). This degradation suggests the splitting of a factor into non-robust artifacts. Therefore, the 6-factor solution was selected as the optimal choice, offering the best balance of chemical resolution and statistical robustness. The average concentration and 1σ variability for the chosen 6-factor solution are presented in Figure S13

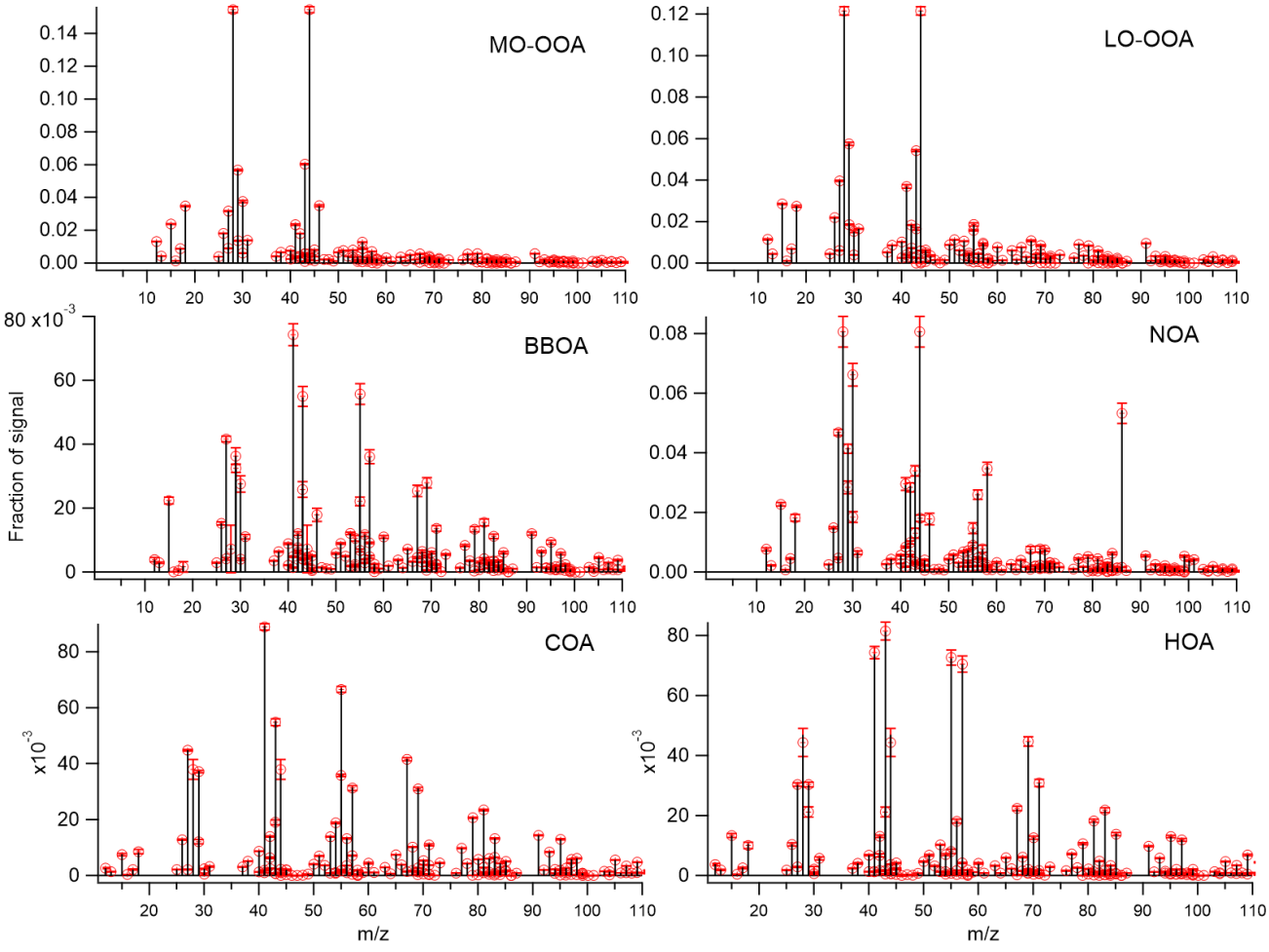

Figure S13. Bootstrapping analysis of the 6-factor solution (average factor with 1σ variation for each point)

References

Kim, H., Zhang, Q., Bae, G.-N., Kim, J.Y., Lee, S.B., 2017. Sources and atmospheric processing of winter aerosols in Seoul, Korea: Insights from real-time measurements using a high-resolution aerosol mass spectrometer. Atmos. Chem. Phys. 17, 2009–2033. https://doi.org/10.5194/acp-17-2009-2017

EPA: EPA Positive Matrix Factorization (PMF) 5.0 Fundamentals and User Guide, U.S. Environmental Protection Agency, 2014. https://www.epa.gov/sites/default/files/2015-02/documents/pmf_5.0_user_guide.pdf

Waked, A., Favez, O., Alleman, L.Y., Piot, C., Petit, J.E., Delaunay, T., Verlinden, E., Jayne, J., Sciare, J., 2014. Source apportionment of PM10 in a north-western Europe regional urban background site (Lens, France) using positive matrix factorization and including primary emissions. Atmos. Chem. Phys. 14, 3325–3346. https://doi.org/10.5194/acp-14-3325-2014

Soleimani, M., Ebrahimi, Z., Mirghaffari, N., Naseri, M., 2022. Source identification of polycyclic aromatic hydrocarbons associated with fine particulate matters (PM2.5) in Isfahan City, Iran, using diagnostic ratio and PMF model. Environ. Sci. Pollut. Res. 29, 30310–30326. https://doi.org/10.1007/s11356-021-17635-8